

# Valley Zeeman Effect in Elementary Optical Excitations of a Monolayer WSe<sub>2</sub>

Ajit Srivastava<sup>1</sup>, Meinrad Sidler<sup>1</sup>, Adrien V. Allain<sup>2</sup>,

Dominik S. Lembke<sup>2</sup>, Andras Kis<sup>2</sup>, and A. Imamoglu<sup>1</sup>

<sup>1</sup>*Institute of Quantum Electronics, ETH Zurich, CH-8093 Zurich, Switzerland and*

<sup>2</sup>*Electrical Engineering Institute, Ecole Polytechnique*

*Federale de Lausanne (EPFL), CH-1015 Zurich, Switzerland.*

\*Correspondence to: imamoglu@phys.ethz.ch, sriva@phys.ethz.ch

**Abstract:** A monolayer of a transition metal dichalcogenide (TMD) such as WSe<sub>2</sub> is a two-dimensional (2D) direct band-gap valley-semiconductor [1, 2] having an effective Honeycomb lattice structure with broken inversion symmetry. The inequivalent valleys in the Brillouin zone could be selectively addressed using circularly-polarized light fields [3–5], suggesting the possibility for magneto-optical measurement and manipulation of the valley pseudospin degree of freedom [6–8]. Here we report such experiments that demonstrate the valley Zeeman effect – strongly anisotropic lifting of the degeneracy of the valley pseudospin degree of freedom using an external magnetic field. While the valley-splitting measured using the exciton transition is consistent with the difference of the conduction and valence band orbital magnetic moments, the trion transition exhibits an unexpectedly large valley Zeeman effect which cannot be understood using an independent electron-hole picture. Instead, we find an explanation using the recently predicted large Berry curvature and the associated magnetic moment for the electron-hole exchange interaction modified trion dispersion [3]. Our results raise the possibility of observing optical excitation induced valley Hall effect in monolayer TMDs or topological states of photons strongly coupled to trion excitations in a microcavity [10].

## Main Text

Charge carriers in two-dimensional (2D) layered materials with a honeycomb lattice, such as graphene and TMDs, have a two-fold valley degree of freedom labelled by  $\pm K$ -points of the Brillouin zone, which are related to each other by time-reversal symmetry [7]. In TMDs, the low

energy physics takes place in the vicinity of  $\pm K$  points of the conduction and valence bands with Bloch states that are formed primarily from  $d_{z^2}$  and  $d_{x^2-y^2}, d_{xy}$  orbitals of the transition metal, respectively [1]. The magnetic moment of charged particles in a monolayer TMD arises from two distinct contributions: the intra-cellular component stems from the hybridization of the  $d_{x^2-y^2}$  and  $d_{xy}$  orbitals as  $d_{x^2-y^2} \pm id_{xy}$ , which provide the Bloch electrons at  $\pm K$  in the valence band an azimuthal angular momentum along  $z$  of  $l_z = \pm 2\hbar$  (Fig. 1a). The second – inter-cellular – contribution originates from the phase winding of the Bloch functions at  $\pm K$ -points [12–15]. In a two-band model, this latter contribution to orbital magnetic moment is identical for conduction and valence bands but much like the intracellular contribution, is opposite in the two valleys.

In a 2D material such as a monolayer TMD, the current circulation from the orbitals can only be within the plane; as a consequence, the corresponding orbital magnetic moment can only point out-of-plane. A magnetic field ( $B$ ) along  $z$  distinguishes the sense of circulation in 2D, causing the opposite energy shifts ( $-\boldsymbol{\mu} \cdot \mathbf{B}$ ) in  $\pm K$  valleys due to opposite magnetic moments. The lifting of degeneracy between the two valleys in presence of  $B$ , represents a valley analogue of the spin Zeeman effect. Optical absorption or emission experiments would allow for a direct determination of this valley Zeeman effect since the valley index ( $\pm K$ ) for independent electron-hole pairs is linked to the helicity of light ( $\sigma^\pm$ ) emitted normal to the monolayer [3–5]. It is well known, on the other hand, that the optical excitation spectra of TMDs are strongly modified by Coulomb interactions, leading to strongly bound neutral and charged exciton resonances. Moreover, it has been recently shown that the electron-hole exchange interaction couples the  $\pm K$  valleys and results in exciton and trion energy dispersion that is vastly different from the single-particle description [3]. It is therefore not a priori clear to what extent the predictions about circular dichroism or orbital magnetic moment that are based on a non-interacting particle picture remain valid in optical measurements.

The samples studied in our experiments were obtained by mechanical exfoliation of WSe<sub>2</sub> synthetic crystals onto heavily doped silicon substrates with 285 nm SiO<sub>2</sub> layer on top [16, 17]. Monolayer flakes were identified using their optical contrast. Polarisation-resolved photoluminescence (PL) and resonant white-light reflection spectroscopy were performed in a home-built confocal microscope setup placed in a liquid helium bath cryostat. The sample temperature was 4.2 K and the excitation source was a helium-neon (HeNe) laser at 632.8 nm or a tunable continuous-wave (cw) Ti:Sapphire laser. The spot size for collection wavelength was  $\sim 1\mu\text{m}$  whereas that for 632.8 nm

was  $\sim 2\text{-}5\ \mu\text{m}$ . Magnetic fields in the range  $\pm 8.4\text{T}$  were applied both parallel and perpendicular to the plane of the sample. The polarisation control of excitation and photoluminescence was done using a liquid crystal retarder calibrated for half and quarter wavelength retardance at exciton and trion wavelengths.

We perform polarisation-resolved photoluminescence (PL) spectroscopy on monolayer  $\text{WSe}_2$  to identify the low energy optical excitations (see Methods). Figure 1b shows a typical polarisation-resolved PL spectra at zero field. A sizeable “valley coherence” or linear dichroism ( $\sim 20\%$ ) of the exciton peak ( $X^0$ ) at  $\sim 708\ \text{nm}$  confirms its monolayer nature [18]. The peak at around  $722\ \text{nm}$  is identified as originating from charged exciton (trion) ( $X^-$ ) emission, consistent with the previous PL studies on  $\text{WSe}_2$  [18]. Polarisation-resolved PL measurements yielded a valley-contrasting circular dichroism of less than  $20\%$  for both  $X^0$  and  $X^-$  resonances in all the flakes that are measured. As we argue below, the electron-hole exchange-induced mixing of the two valleys is possibly responsible for reducing the degree of circular dichroism [3].

Figure 2a shows the behaviour of  $X^0$  at various  $B$  up to  $8.4\ \text{T}$  in the Faraday geometry ( $B \parallel z$ ). The PL is analysed in a circularly polarised basis while the excitation of the laser is kept linearly polarised, detuned by over  $200\ \text{meV}$  from the  $X^0$  resonance. A clear splitting of the  $X^0$  peak as a function of  $B$  is observed: the splitting increases linearly with  $B$  with slope of about  $0.25\ \text{meV/T}$  (Fig. 2b). The magnitude of  $B$ -dependent splitting in 5 different flakes are observed to be within  $\pm 10\%$  of this value. We have also carried out resonant reflection measurements showing a similar yet slightly smaller splitting of  $\sim 0.21\ \text{meV/T}$  for the exciton line (Fig. 2c). The fact that we do not observe the trion peak in reflection measurements indicate that our sample has a low doping density.

The measurement of the magnetic-field dependence of PL in Voigt geometry ( $B \perp z$ ) shows no observable splitting up to the highest  $B$  (Fig. 3a). This extreme anisotropy in the magnetic response of the monolayer is a direct consequence of the fact that the orbital magnetic moment of a strictly 2D material points out-of-plane and thus can only couple to  $B_z$ . This observation also rules out a spin-Zeeman contribution to the measured splitting. Although the shift due to spin-Zeeman effect has opposite signs in the two valleys, it is particle-hole symmetric in each valley and therefore does not contribute to the splitting of optical transitions, much like the intercellular orbital magnetic moment (Fig. 2d). As expected, if the direction of  $B$  in Faraday geometry is reversed, the helicity of the split peaks also switches (Fig. 3b).

When the B-dependent PL data is analysed in linear basis no clearly resolvable splitting is observed (Fig. 3c); this is a consequence of the fact that the split  $X^0$  lines are circularly polarised and have a linewidth that is larger than the maximum attainable B-field induced splitting. By varying the polarisation setting of both the excitation laser and the detection, it is confirmed that for finite  $B$  the split peaks are of opposite circular polarisation irrespective of the polarisation of the excitation laser. Upon linearly polarised excitation and circularly polarised detection, the intensities of the two split peak is found to be about the same.

The observation of a splitting in the circularly-polarised basis that scales linearly with the applied  $B$  field is consistent with an independent electron-hole description, as well as that of electron-hole-exchange mediated coupling between the excitonic excitations in the  $\pm K$  valleys. In both models, the lifting of the degeneracy occurs due to the equal but opposite orbital magnetic moment of the two valleys together with unequal orbital magnetic moments of conduction and valence bands within the same valley, as shown in Fig 2d. For excitations with a vanishing in-plane momentum, optical transition in each valley experiences a shift in energy which is linear in  $B$ , given by  $\delta E_{\pm K} = -(\boldsymbol{\mu}_c - \boldsymbol{\mu}_v) \cdot \mathbf{B} = (\mu_{\pm K,v} - \mu_{\pm K,c})B_z$  where  $\mu_{-K,v(c)} = -\mu_{K,v(c)}$  are the sum of the intra- and inter-cellular orbital magnetic moments of the valence (conduction) bands in the two valleys. Clearly, a necessary requirement for observing splitting in optical transitions is electron-hole symmetry breaking.

The magnitude of intra-cellular orbital magnetic moment of valence band in the two valleys is  $\mu_v = (e/2m)l_z = 2\mu_B$ , where  $\mu_B = e\hbar/2m_e$  is the Bohr magneton. With this, one can estimate the magnitude of the splitting arising purely from the magnetic moment of the  $d$ -orbitals or the intra-cellular contribution as  $\Delta_{K,-K}^{intra} = (2\mu_B - (-2\mu_B))B_z = 4\mu_B B_z$ . In a particle-hole symmetric, two-band model, the values of inter-cellular orbital magnetic moment are the same for conduction and valence band, leading to a vanishing contribution to the splitting of optical transition between the bands. TMDs break particle-hole symmetry and a three-band model is needed to capture the band structure near the  $\pm K$  points as was recently shown [1]. We calculate the intercellular orbital magnetic moment for the two bands using the three-band tight binding parameters for WSe<sub>2</sub> [1] and find them to be comparable in magnitude to the intra-cellular magnetic moment of the valence band (Supplementary Materials S1). However, their difference is much smaller and should only have a minor contribution to the splitting of optical transition. Indeed, the observed splitting of about  $4.3 \mu_B B_z$  agrees well with the intracellular contribution from the  $d$ -orbitals. Nevertheless,

we emphasize that in contrast to our experimental findings, the three-band model suggests that the finite inter-cellular contribution should reduce the value of the splitting to about  $3.3 \mu_B B_z$ .

Figure 4a shows the polarisation dependent PL spectra of  $X^-$  as a function of  $B$  in the Faraday geometry. Much like the  $X^0$  peak, a splitting of the two circularly polarised components of PL is observed, which increases linearly with  $B$  in Faraday geometry. As in the exciton case, the Voigt geometry measurements did not yield any measurable splitting. Surprisingly however, the magnitude of  $X^-$  splitting was measured to be significantly larger than that of  $X^0$  peak in all the flakes that were studied. As shown in Fig. 4b, the splitting scales linearly with  $B$  with a slope of  $\sim 0.32 - 0.36$  meV/T which is more than 25% larger than that of the  $X^0$  peak.

A negatively (positively) charged trion is a three-body correlated state comprising of a photo-generated electron-hole pair which binds with an electron (hole) in the conduction (valence) band. The binding energy of this three-body state is  $\sim 30$  meV, as determined from the red-shift of  $X^-$  peak from the  $X^0$  resonance. The PL peak of  $X^-$  arises from an optical transition in which the initial state is that of the trion while the final state has a Bloch electron in the conduction band. Since  $B$ -dependent PL splitting is determined by the difference in the orbital magnetic moment between the initial and final states of the optical transition, one expects the  $B$ -dependent  $X^0$  and  $X^-$  PL splittings to be identical, since the extra electron in the trion should contribute identically to the initial and the final state magnetic moment. This simple non-interacting picture is clearly inconsistent with our experimental findings and strongly suggests the role of interactions in determining the magnetic moment of trions.

Indeed, the degeneracy of the two trion states with center-of-mass momentum  $K$  ( $-K$ ) that are comprised of an electron in  $K$  ( $-K$ ) valley and a bright exciton occupying either the same or the opposite valley, is lifted by the electron-hole exchange interaction. The absence of valley coherence of  $X^-$  peak in monolayer WSe<sub>2</sub> has been attributed to the fast phase-rotation associated with this energy splitting [18]. Recently, it was theoretically shown that the corresponding exchange-induced modification of the trion dispersion ensures that the trion states with center-of-mass momentum  $\sim \pm K$  carry a large Berry curvature [3]. If the trion can be considered as a strongly bound, charged quasi-particle, the exchange-induced Berry curvature  $\Omega(k)$  will be accompanied by a contribution to the orbital magnetic moment that is given by  $\mu(k) = \frac{e}{2\hbar} \Omega(k) \delta_{ex}$  for  $k \simeq \pm K$ ; here  $\delta_{ex}$  is the exchange-induced splitting of the trion resonances. Since this additional contribution to the orbital magnetic moment exists only in the initial state of optical emission, it could explain the

larger splitting of  $X^-$  transition as compared to  $X^0$  in our experiments (Fig. 4c), provided that the  $X^-$  PL originates mainly from the lower trion branch where the exciton and the additional electron occupy the same valley. In order to estimate the magnitude of splitting based on this additional contribution to magnetic moment, one needs to know the range of momenta of trion involved in the radiative recombination and the Thomas-Fermi vector corresponding to the carrier screening. In the absence of this information, we refrain from making a quantitative estimate of the expected trion splitting (Supplementary Materials S2). It should be noted that this unique exchange-induced contribution to the magnetic moment is very similar to the intercellular contribution in that it stems from the non-trivial geometry of the trion band-structure; however, it is optically induced and only exists within the lifetime of trion.

Another expected experimental signature of the electron-hole exchange interaction that acts as an exciton momentum-dependent effective in-plane magnetic field for the valley pseudospin [3], is a reduction of the circular dichroism. An out-of-plane  $B$  lifts the valley degeneracy and should, in principle, overcome the valley-mixing due to exchange thereby increasing the circular dichroism. Our measurements (Fig. 3d) show a sizeable increase of the degree of circular dichroism by a factor of 1.7 - 2 at  $B = 8.4$  T as compared to its zero field value and are qualitatively consistent with this prediction. However, a quantitative estimation of this increase is not easy as it depends on the details of relaxation processes following a non-resonant excitation in a PL experiment.

While the observation of valley Zeeman effect from the exciton emission validates the predicted 2D band structure of TMDs and establishes the valley degree of freedom as a pseudospin index; the anomalous  $B$ -dependent splitting of the trion emission opens up exciting possibilities since it shows that the elementary properties of these 2D semiconductors, such as the magnetic moment and the Berry curvature could be modified by photon absorption or emission. In addition, the exchange-induced Berry curvature of trions should make the valley Hall effect easier to measure as compared to an experiment based on excitons since no ionisation of optically generated electron-hole pair is needed [19]. An interesting direction to pursue would be to couple a TMD monolayer to the photonic modes of a high quality-factor cavity and to use the exchange coupling of the trion states to create topological states of trion-polaritons, as was recently proposed [10].

During the preparation of the manuscript, we became aware of similar results by the University of Washington group [20] and the Cornell group [21].

- 
- [1] Mak, K. F., Lee, C., Hone J., Shan J. & Heinz, T. F. Atomically Thin MoS<sub>2</sub>: A New Direct-Gap Semiconductor. *Phys. Rev. Lett.* **105**, 136805 (2010).
- [2] Splendiani, A. *et al.* Emerging photoluminescence in monolayer MoS<sub>2</sub>. *Nano Lett.* **10**, 1271 (2010).
- [3] Cao, T. *et al.* Valley-selective circular dichroism of monolayer molybdenum disulphide. *Nat. Commun.* **3**, 887 (2012).
- [4] Zeng, H., Dai, J., Yao, W., Xiao, D. & Cui, X. Valley polarization in MoS<sub>2</sub> monolayers by optical pumping. *Nat. Nanotech.* **7**, 490-493 (2012).
- [5] Mak, K. F., He, K., Shan, J. & Heinz, T. F. Control of valley polarization in monolayer MoS<sub>2</sub> by optical helicity. *Nat. Nanotech.* **7**, 494-498 (2012).
- [6] Di, X., Chang, M.-C., Niu, Q. Berry phase effect on electronic properties. *Rev. Mod. Phys.* **82**, 1959 (2010).
- [7] Xiao, D., Liu, G.-B., Feng, W., Xu, X. & Yao, W. Coupled Spin and Valley Physics in Monolayers of MoS<sub>2</sub> and Other Group-VI Dichalcogenides. *Phys. Rev. Lett.* **108**, 196802 (2012).
- [8] Xu, X., Wang, Y., Di, X., Heinz, T. F. Spins and Pseudospins in layered transition metal dichalcogenides. *Nat. Phys.* **10**, 343-350 (2014).
- [9] Yu, H., Liu, G.-B., Gong, P., Xu, X. & Yao, W. Dirac cones and Dirac saddle points of bright excitons in monolayer transition metal dichalcogenides. *Nat. Commun.* **5**, 3876 (2014).
- [10] Karzig, T., Bardyn, C.-E., Lindner, N. & Refael, G. Topological polaritons from quantum wells in photonic waveguides or microcavities. *arXiv:1406.4156v1* (2014).
- [11] Liu, G.-B., Shan, W.-Y., Yao, Y., Yao, W. & Xiao, D. Three-band tight-binding model for monolayers of group-VIB transition metal dichalcogenides. *Phys. Rev. B* **88**, 085433 (2013).
- [12] Thonhauser, T., Ceresoli, D., Vanderbilt, D., & Resta, R. Orbital Magnetization in Periodic Insulators. *Phys. Rev. Lett.* **95**, 137205 (2005).
- [13] Ceresoli, D., Thonhauser, T., Vanderbilt, D., & Resta, R. Orbital magnetization in crystalline solids: Multi-band insulators, Chern insulators, and metals. *Phys. Rev. B.* **74**, 024408 (2006).
- [14] Xiao, D., Yao, W. & Niu, Q. Valley-contrasting physics in graphene: Magnetic moment and topological transport. *Phys. Rev. Lett.* **99**, 236809 (2007).
- [15] Yao, W., Xiao, D. & Niu, Q. Valley-dependent optoelectronics from inversion symmetry breaking. *Phys. Rev. B* **77**, 235406 (2008).
- [16] Novoselov, K. S. *et al.* Two-dimensional atomic crystals. *Proc. Natl Acad. Sci. USA* **102**, 10451-10453 (2005).

- [17] Radisavljevic, B., Radenovic, A., Brivio, J., Giacometti, V. & Kis, A. Single-layer MoS<sub>2</sub> transistors. *Nat. Nanotech.* 6, 147-150 (2011).
- [18] Jones, A. M. *et al.* Optical Generation of Excitonic Valley Coherence in Monolayer WSe<sub>2</sub>. *Nat. Nanotech.* 8, 896-869 (2013).
- [19] Mak, K. F., McGill, K. L., Park, J. & McEuen, P. L. The valley Hall effect in MoS<sub>2</sub> transistors. *Science* 344, 14896-1492 (2014).
- [20] Aivazian, G. *et al.* Magnetic control of valley pseudospin in monolayer WSe<sub>2</sub>. *Submitted* (2014).
- [21] MacNeill, D. *et al.* Valley degeneracy breaking by magnetic field in monolayer MoSe<sub>2</sub>. *arXiv:1407.0686v1* (2014).

**Acknowledgments** We acknowledge many enlightening discussions with Wang Yao, particularly regarding the role of intra-cellular current and the electron-hole exchange in optical excitations in TMDs. This work is supported by NCCR Quantum Science and Technology (NCCR QSIT), research instrument of the Swiss National Science Foundation (SNSF)



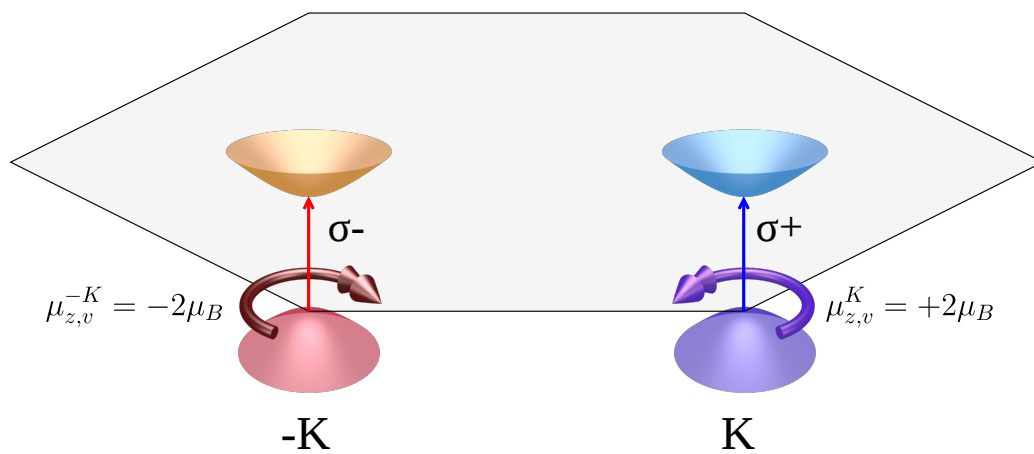
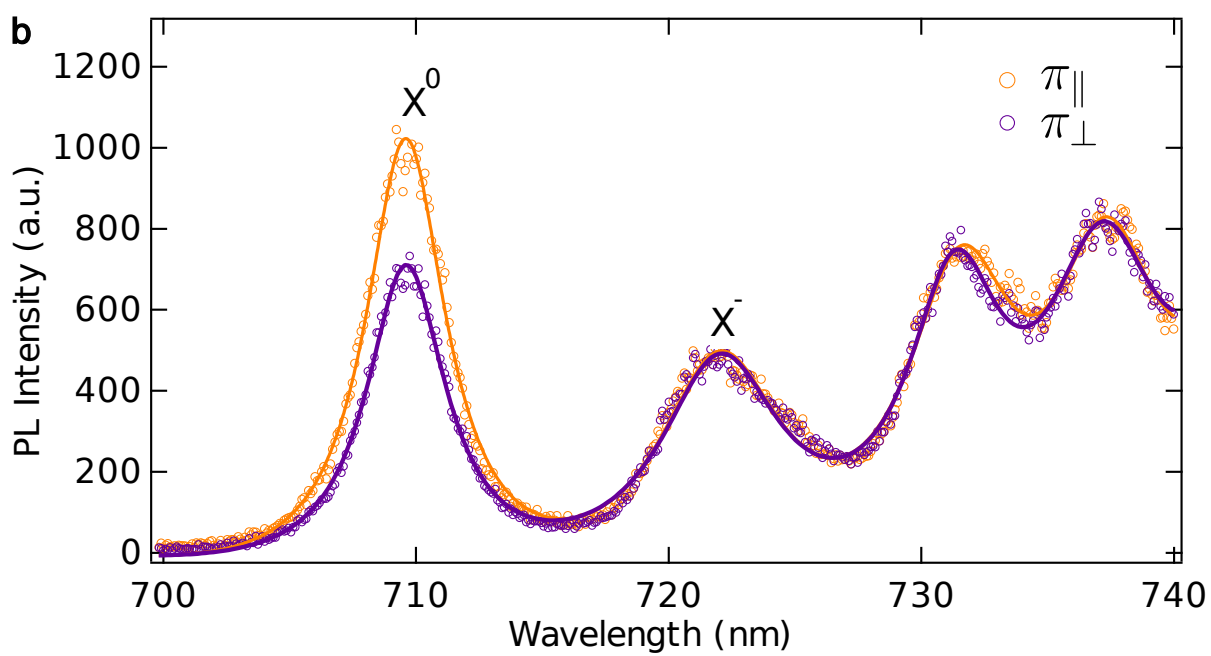
**Figure 1: Photoluminescence of a monolayer WSe<sub>2</sub>.** **a**, A schematic description of the band structure showing the valley dependent intra-cellular circulation of the valence band electrons. The double circulating clockwise (counter-clockwise) arrow denotes the out-of-plane orbital magnetic moment of  $+2 \mu_B$  ( $-2 \mu_B$ ) arising from  $d + id$  ( $d - id$ ) orbitals in the valence band at  $K$  ( $-K$ ) valley. The conduction band formed out of  $d_{z^2}$  orbital carries no such magnetic moment. **b**, A typical photoluminescence (PL) spectra at 4.2 K showing the neutral exciton ( $X^0$ ) and negatively charged exciton or trion ( $X^-$ ) resonance at around 708 nm and 722 nm, respectively. The laser polarisation is linear and the PL is detected co-polarised (orange) or cross-polarized (purple) to it, showing linear dichroism only for the  $X^0$  peak.

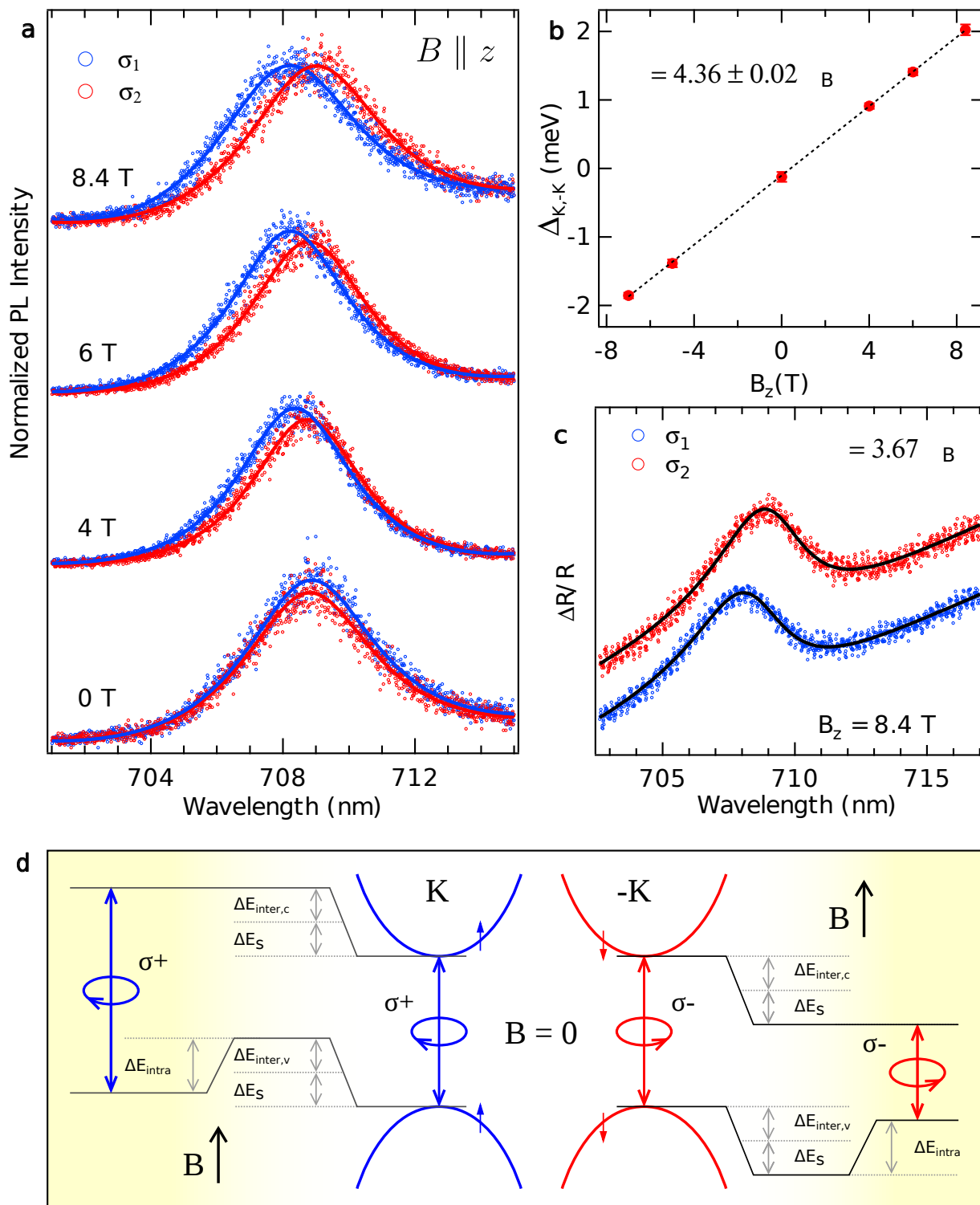
**Figure 2: Magnetic field dependence of exciton photoluminescence and the valley Zeeman effect** **a**, Normalised polarisation-resolved photoluminescence (PL) spectra of the neutral exciton ( $X^0$ ) peak as a function of the out-of-plane magnetic field ( $B$ ). The excitation laser is polarised linearly while the red and blue traces correspond to PL analysed in circularly polarised basis. The spectra at different  $B$  are normalised to the zero field data while that at the same  $B$  are unnormalised. The solid lines are fit to the data. The  $B$  dependent splitting results from valley Zeeman effect as depicted in **d**. **b**, Splitting extracted from fits in **a** showing linear increase with  $B$ . Dashed line is a linear fit to the data. **c**, Resonant differential reflectance spectra at +8.4 T obtained using a filtered white light source. Solid black lines are fits to the data using an admixture of absorptive and dispersive lineshapes. **d**, Valley Zeeman effect - In a finite out-of-plane  $B$ , the degeneracy between the  $\pm K$  valleys is lifted due to contributions from spin Zeeman effect ( $\Delta E_s$ ), the intercellular orbital magnetic moment ( $\Delta E_{\text{inter}}$ ), and the intracellular contribution from the  $d \pm id$  orbitals of the valence band ( $\Delta E_{\text{intra}}$ ). The signs of these contributions are opposite in the two valleys.  $\Delta E_s$  and  $\Delta E_{\text{inter}}$  for a 2-band model cause equal energy shifts of the conduction and the valence band hence can not be detected in PL. The resulting valley-split transitions are circularly polarised.

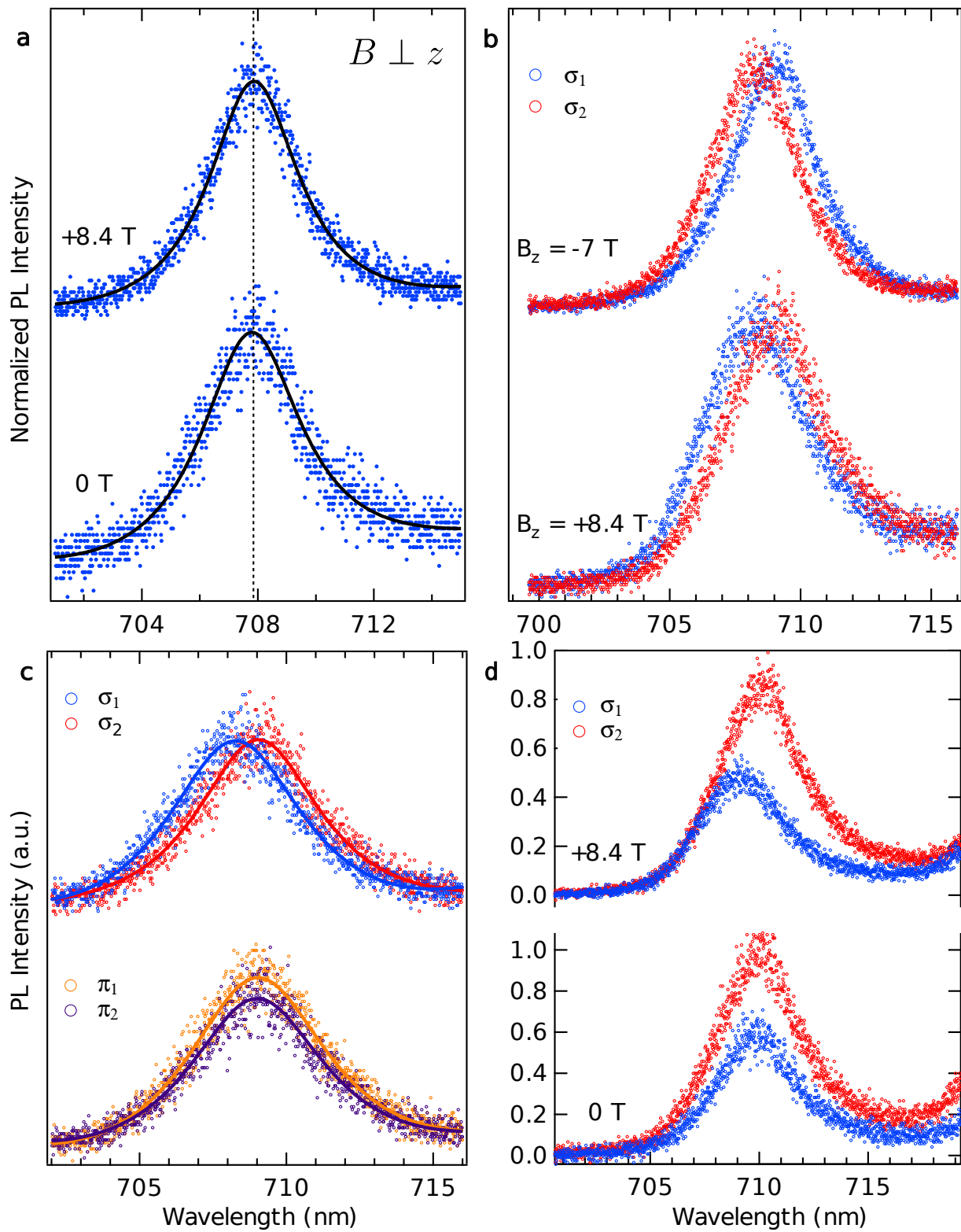
**Figure 3: Strongly anisotropic magnetic response of photoluminescence and its polarisation dependence.** **a**, Exciton photoluminescence spectra as a function of in-plane magnetic field  $B$  (Voigt geometry) showing no observable splitting even at the highest applied field of 8.4 T. The dotted line depicts the emission center wavelength which is identical for 0 T

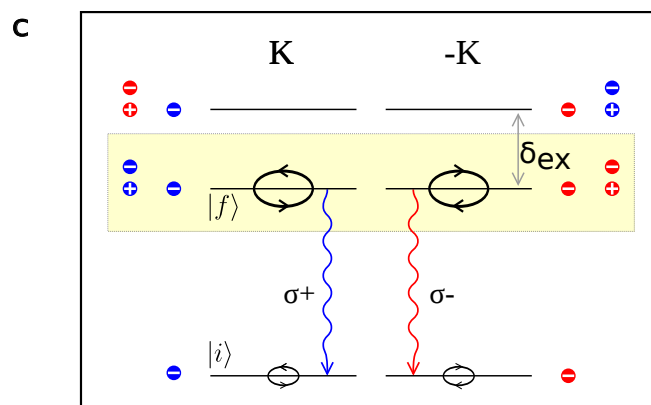
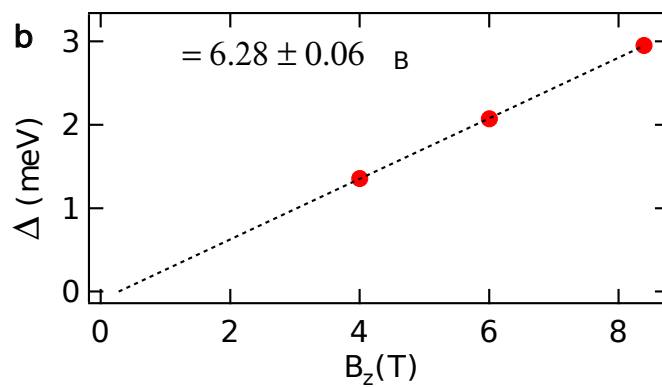
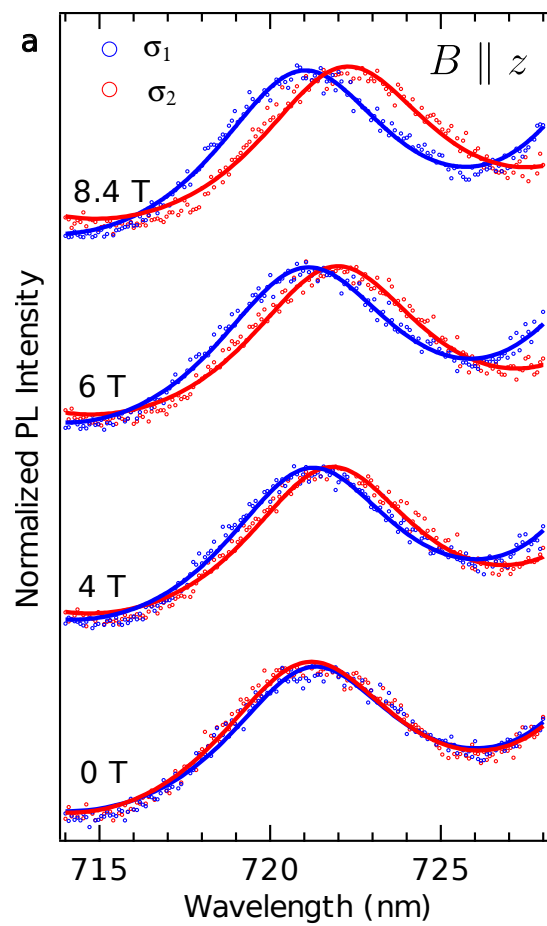
and 8.4 T. **b**, Polarity reversal of  $B$  leads to switching of the emission helicity of the two peaks together with a sign change of the splitting, consistent with the valley Zeeman effect depicted in Fig. 2d. **c**, Polarisation dependence of magnetic splitting at 8.4 T showing no clear splitting when the photoluminescence is analysed in the linear basis, confirming that the split peaks are circularly polarised. **d**, Circular dichroism as a function of out-of-plane magnetic field shows a clear increase by about a factor of 2. The out-of-plane  $B$  can overcome the valley-mixing due to electron-hole exchange interaction leading to the observed increase.

**Figure 4: Magnetic field dependence of trion photoluminescence.** **a**, Normalised polarisation-resolved photoluminescence (PL) spectra of the trion ( $X^-$ ) peak as a function of out-of-plane magnetic field ( $B$ ). **b**, Linear fit to the splitting extracted from **a** as function of  $B$  gives a larger value of the trion orbital magnetic moment as compared to the exciton (Fig. 2b). **c**, An illustration of the different orbital magnetic moments of initial  $|i\rangle$  and final states  $|f\rangle$  in  $X^-$  optical emission process. The blue (red) symbols label the  $K$  ( $-K$ ) valley. The electron-hole exchange energy ( $\delta_{ex}$ ) splits the trion dispersion into lower and upper branches with the excess electron and the exciton occupying the same valley or the opposite. We assume that the radiative recombination occurs predominantly from the same-valley branch with lower energy. The initial state of the optical emission is thus a trion with exchange-induced magnetic moment while the final state is a Bloch electron in the conduction band with an orbital magnetic moment given by the intercellular circulation. The difference between the two magnetic moments is finite and adds to the intracellular contribution.

**a****b**







**Supplementary Information:**

**S1. Intercellular orbital magnetic moment in three-band tight binding model of WSe<sub>2</sub>**

As mentioned in the main text, the intercellular contribution to the orbital magnetic moment in a two-band model is identical for conduction and valence band. However, this particle-hole symmetry is broken in TMDs and one can expect a finite difference between the intercellular orbital magnetic moment of the conduction and the valence band. We use the three-band tight binding model of Liu *et al.* [1] to calculate the difference in orbital moments of the two bands. Eq. 4 of Liu *et al.* publication presents a Hamiltonian which captures the band-structure of TMDs around  $\pm K$ -points  $(\pm \frac{4\pi}{3a}, 0)$  -

$$H(\mathbf{k}) = \begin{pmatrix} h_0 & h_1 & h_2 \\ h_1^* & h_{11} & h_{12} \\ h_2^* & h_{12}^* & h_{22} \end{pmatrix}.$$

We begin by expanding  $H(k)$  at  $K$ -point to first order in  $k_x$  and  $k_y$ ,

$$h_0 = \epsilon_1 - 3t_0 \tag{1}$$

$$h_1 = -\frac{3}{2} \left( \sqrt{3}t_2k_ya + it_1k_xa \right) \tag{2}$$

$$h_2 = \frac{3}{2} \left( \sqrt{3}t_2k_xa + it_1k_ya \right) \tag{3}$$

$$h_{11} = \left( -\frac{3}{2} + \frac{3\sqrt{3}}{4}k_xa \right) t_{11} + \left( -\frac{3}{2} - \frac{3\sqrt{3}}{4}k_xa \right) t_{22} + \epsilon_2 \tag{4}$$

$$h_{22} = \left( -\frac{3}{2} + \frac{3\sqrt{3}}{4}k_xa \right) t_{22} + \left( -\frac{3}{2} - \frac{3\sqrt{3}}{4}k_xa \right) t_{11} + \epsilon_2 \tag{5}$$

$$h_{12} = \frac{3\sqrt{3}}{4}k_ya(t_{22} - t_{11}), \tag{6}$$

where the parameters  $a$ ,  $\epsilon_1$ ,  $\epsilon_2$ ,  $t_0$ ,  $t_1$ ,  $t_2$ ,  $t_{11}$ ,  $t_{22}$ , and  $t_{12}$  are to be taken from Table II of Liu *et al.* It is convenient to make the above Hamiltonian traceless by choosing the energy datum as  $\frac{1}{3}\text{Tr}(H)$ . The Hamiltonian then reduces to -

$$\tilde{H}(k_x, k_y) = \begin{pmatrix} -2c & -vak_y - iuak_x & vak_x - iuak_y \\ -vak_y + iuak_x & c + dak_x & -dak_y - iw \\ vak_x + iuak_y & -dak_y + iw & c - dak_x \end{pmatrix}, \tag{7}$$

where,

$$c = \frac{(\epsilon_2 - \epsilon_1)}{3} - \frac{1}{2}(t_{11} + t_{22} - 2t_0) \quad (8)$$

$$u = \frac{3}{2}t_1 \quad (9)$$

$$v = \frac{3\sqrt{3}}{2}t_2 \quad (10)$$

$$w = 3\sqrt{3}t_{12} \quad (11)$$

$$d = \frac{3\sqrt{3}}{4}(t_{11} - t_{22}). \quad (12)$$

At  $K$ -point, the eigenvalues are -

$$E_1 = c - w \quad \text{valence band} \quad (13)$$

$$E_2 = -2c \quad \text{conduction band} \quad (14)$$

$$E_3 = c + w \quad \text{higher band.} \quad (15)$$

The corresponding eigenvectors are  $u_1 = \frac{1}{\sqrt{2}}(0, i, 1)^T$ ,  $u_2 = (1, 0, 0)^T$  and  $u_3 = \frac{1}{\sqrt{2}}(0, -i, 1)^T$  which in the basis  $\{|d_{z^2}\rangle, |d_{x^2-y^2}\rangle, |d_{xy}\rangle\}$  confirm that the valence band at  $K$ -point is formed out of  $\frac{1}{\sqrt{2}}(|d_{x^2-y^2}\rangle + i|d_{xy}\rangle)$  orbital while the conduction band is made solely from  $|d_{z^2}\rangle$  orbital, within this three-band model.

From Eq. 7, one easily calculates  $\partial\tilde{H}/\partial k_x$  and  $\partial\tilde{H}/\partial k_y$  at  $K$  to be -

$$\left. \frac{\partial\tilde{H}}{\partial k_x} \right|_{\mathbf{K}} = \begin{pmatrix} 0 & -iua & va \\ iua & da & 0 \\ va & 0 & -da \end{pmatrix}, \quad (16)$$

and

$$\left. \frac{\partial\tilde{H}}{\partial k_y} \right|_{\mathbf{K}} = \begin{pmatrix} 0 & -va & -iua \\ -va & 0 & -da \\ iua & -da & 0 \end{pmatrix}, \quad (17)$$

The orbital angular momentum  $L_n(k)$  for the  $n$ -th band is given by the following expression [2, 4],

$$L_n(k) = i\frac{m}{\hbar} \sum_{j \neq n} \left[ \frac{\langle u_{n,k} | \frac{\partial H}{\partial k_x} | u_{j,k} \rangle \langle u_{j,k} | \frac{\partial H}{\partial k_y} | u_{n,k} \rangle}{E_j - E_n} - \text{c.c} \right], \quad (18)$$

yielding -

$$L_1(\mathbf{K}) = -\frac{m}{\hbar} a^2 \left( \frac{(u+v)^2}{3c-w} + \frac{d^2}{w} \right) \quad (19)$$

$$L_2(\mathbf{K}) = -\frac{m}{\hbar} a^2 \frac{2w(u^2 + v^2) + 6cuv}{(9c^2 - w^2)}. \quad (20)$$



The orbital magnetic moment for the  $n$ -th band is then  $\mu_n(k) = \frac{e}{2m} L_n(k)$ . Plugging the numbers for the parameters, we get -

$$\mu_{v,inter}(\mathbf{K}) = 3.49 \mu_B \quad (\text{GGA}) \quad (21)$$

$$\mu_{c,inter}(\mathbf{K}) = 3.83 \mu_B \quad (\text{GGA}) \quad (22)$$

$$\mu_{v,inter}(\mathbf{K}) = 3.41 \mu_B \quad (\text{LDA}) \quad (23)$$

$$\mu_{c,inter}(\mathbf{K}) = 3.75 \mu_B \quad (\text{LDA}) \quad (24)$$

The total orbital magnetic moment at  $K$ -point then becomes  $\mu_{tot} = \mu_{inter} + \mu_{intra}$ , yielding a splitting of  $3.34 \mu_B B_z$  (GGA) and  $3.32 \mu_B B_z$  (LDA).

## S2. Orbital magnetic moment of trion in WSe<sub>2</sub> due to finite Berry curvature

According to Yu *et al.* [3], the trion ( $X^-$ ) dispersion near  $\pm K$ -point has an exchange-induced gap of  $\delta_{ex}$  which results in a large Berry curvature,  $\Omega_{X^-}(k)$ . If we treat  $X^-$  as a charged quasi-particle described by a two-band model of Yu *et al.* near  $\pm K$ -points, the finite Berry curvature is accompanied by an orbital angular momentum  $L(k)$  which is identical for both bands. Using Eq. 18 of S1, we get  $L(\mathbf{k})$  as,

$$L(\mathbf{k}) = i \frac{m}{\hbar} \left[ \frac{\langle u_{1,k} | \frac{\partial H}{\partial k_x} | u_{2,k} \rangle \langle u_{2,k} | \frac{\partial H}{\partial k_y} | u_{1,k} \rangle}{E_g(k)} - \text{c.c} \right]. \quad (25)$$

where  $E_g(k) = \delta_{ex} \left( 1 + \frac{4J^2 k^4}{K^2 \delta_{ex}^2 (k + k_{TF})^2} \right)^{1/2}$  is the  $k$ -dependent gap. Expressing in terms of  $\Omega_{X^-}(k)$ ,

$$L(k) = \frac{m}{\hbar} E_g(k) \Omega_{X^-}(k). \quad (26)$$

The trion magnetic moment is then given by  $\mu_{X^-} = \frac{e}{2m} L(k)$ ,

$$\mu_{X^-}(k) = \frac{eJ^2}{\hbar K^2 \delta_{ex}} \frac{k^2(k + 2k_{TF})}{(k + k_{TF})^3} \left( 1 + \frac{4k^4 J^2}{(k + k_{TF})^2 K^2 \delta_{ex}^2} \right)^{-1} \quad (27)$$

where  $J$  is the electron-hole exchange coupling strength and  $k_{TF}$  is the Thomas-Fermi wavevector corresponding to carrier screening. Fig. S1(a) shows  $\mu(k)$  in units of  $\mu_B$  for  $k$  up to  $0.01K$  and three different values of  $k_{TF}$ . A  $k_{TF}$  of  $0.1 \omega_0/c$  corresponds to a charge density of  $\sim 10^9 \text{ cm}^{-2}$ .

The average (intercellular) magnetic moment depends on the range of  $k$ -wavevectors involved in the radiative recombination and the carrier doping density through  $k_{TF}$ . It can be calculated by averaging over certain wave vector range  $\delta k$ , say from 0 to  $k_{lim}$ . This is shown in Fig. S1(b) for different values of  $k_{TF}$  and different values of  $k_{lim}$  (from  $k_{ph} = \omega_0/c$  to  $0.03K$ ).

In order to observe a splitting of 5.5 to 6.2  $\mu_B$  the trion final state intercellular magnetic moment should be between 4.55 and 4.9  $\mu_B$  since the intracellular contribution to orbital magnetic moment is  $\mu_{intra} = 2\mu_B$ , and the intercellular magnetic moment for the initial state of an electron in the conduction band was estimated to be  $\sim 3.8 \mu_B$  (see supplementary S1). This interval of  $\mu_{avg}$  is shown as white band in Fig. S1(b). It is evident that a wide of range of parameters can lead to the experimentally observed trion splitting.

- 
- [1] Liu, G.-B. *et al.* Three-band tight-binding model for monolayers of group-VIB transition metal dichalcogenides. *Phys. Rev. B* **88**, 085433 (2013).
  - [2] Chang, M.-C. *et al.* Berry phase, hyperorbits, and the Hofstadter spectrum: Semiclassical dynamics in magnetic Bloch bands. *Phys. Rev. B* **53**, 7010 (1996).
  - [3] Yu, H. *et al.* Dirac cones and Dirac saddle points of bright excitons in monolayer transition metal dichalcogenides. *Nat. Commun.* **5**, 3876 (2014).
  - [4] Yafet, Y. *Solid State Physics:Advances in Research and Applications Vol. 14* (Academic, New York, 1963).

**Figure S1: Orbital magnetic moment of trion arising from large Berry curvature.**

**a**, Momentum-resolved orbital magnetic moment of trion ( $X^-$ ) as a function of  $X^-$  centre of mass wavevector  $k$  measured from the  $K$ -point for different Thomas-Fermi wave vectors ( $k_{TF}$ ) of carrier doping densities. **b**, Average magnetic moment of  $X^-$  for a range of wavevectors involved in radiative recombination ( $\delta k$ ) and  $k_{TF}$ . The white band depicts the range of magnetic moments consistent with the experimentally observed trion splitting.

